Structure and Phase Stability of $Ga_xIn_{1-x}P$ Solid Solutions from Computational Alchemy

Nicola Marzari,[1] Stefano de Gironcoli,[2,*] and Stefano Baroni[3]
[1]*Cavendish Laboratory, University of Cambridge, Madingley Road, Cambridge CB3 0HE, United Kingdom*
[2]*Forum di Fisica Teorica dell'Istituto Nazionale di Fisica della Materia, Scuola Normale Superiore, Piazza dei Cavalieri 7, I-56126 Pisa, Italy*
[3]*Scuola Internazionale Superiore di Studî Avanzati (SISSA), Via Beirut 2/4, I-34014 Trieste, Italy*
(Received 16 December 1993)

The structural and thermodynamical properties of $Ga_xIn_{1-x}P$ solid solutions are studied using Monte Carlo simulations based on density-functional perturbation theory. The free-standing alloy displays a model random behavior, with a miscibility gap below $\sim$ 820 K. In samples grown on a GaAs (001) substrate, the resulting epitaxial strain stabilizes various ordered phases which give rise to a rich phase diagram below $\sim$ 230 K. Among these phases, the chalcopyrite is dominant for $x = 0.5$, and two new, more complex, stable phases have been identified at different concentrations.

PACS numbers: 61.66.Dk, 64.70.Kb, 81.30.Bx

In recent years semiconductor solid solutions have attracted much interest due to the flexibility that they offer, upon variation of their composition, in the tuning of their physical properties outside the narrow range otherwise provided by elemental and binary semiconductors. According to the current picture, the phase diagram of these systems is mainly determined by the large elastic energy required to mix lattice-mismatched semiconductors, which drives the tendency for the resulting alloy to segregate and is therefore responsible for the opening of a *miscibility gap* below a certain critical temperature.

A vast amount of evidence has been gathered recently, challenging this simple picture and recording the appearance of *spontaneous ordering* in semiconductor alloys grown by epitaxial techniques [1]. The role of strain in stabilizing some ordered structures was soon recognized [2], but there is now a general consensus on the fact that the mechanisms responsible for the observed structures are to be searched for in surface and/or kinetic effects [3] rather than in bulk thermodynamical stability. Nevertheless, a thorough understanding of the equilibrium properties of these systems is a prerequisite for any further theoretical insight, and much effort has been devoted to their study from first principles [4,5].

The issue of the phase stability of $Ga_xIn_{1-x}P$ is addressed here using the recently developed method of *computational alchemy* [5]. This system is a paradigmatic example of a polar, lattice-mismatched semiconductor alloy, whose interest derives both from its optoelectronic applications and from the clear evidence of the occurrence of unexpected ordering in epitaxially grown samples [6]. The key idea underlying computational alchemy is to consider any actual realization of the solid solution as a slight deviation from a suitably defined reference periodic system—the *virtual crystal*—and to treat it by density-functional perturbation theory (DFPT). In the case of the $Ga_xIn_{1-x}P$ pseudobinary alloy, disorder affects only one of the two fcc sublattices of a zinc blende structure. Let us indicate the knots of such sublattice by $\{\mathbf{R}\}$: a microscopic configuration of the alloy is fully specified by a set of Ising-like variables $\{\sigma_{\mathbf{R}}\}$, defined as $\sigma_{\mathbf{R}} = +1$ if the $\mathbf{R}$ lattice site is occupied by a Ga atom, and $\sigma_{\mathbf{R}} = -1$ if it is occupied by an In atom. For any given configuration and neglecting lattice relaxation for the present, the *bare* alloy potential acting on the valence electrons reads

$$V(\mathbf{r}) = \sum_{\mathbf{R}} v_{\mathrm{P}}(\mathbf{r}-\mathbf{R}-\boldsymbol{\delta}) + \sum_{\mathbf{R}} \frac{1}{2}[v_{\mathrm{Ga}}(\mathbf{r}-\mathbf{R}) + v_{\mathrm{In}}(\mathbf{r}-\mathbf{R})] + \sum_{\mathbf{R}} \sigma_{\mathbf{R}} \frac{1}{2}[v_{\mathrm{Ga}}(\mathbf{r}-\mathbf{R}) - v_{\mathrm{In}}(\mathbf{r}-\mathbf{R})], \quad (1)$$

where $v_{\mathrm{Ga,In,P}}$ are the ionic pseudopotentials of the three atomic species and $\boldsymbol{\delta} = \frac{a_0}{4}(1,1,1)$ is the displacement between the two sublattices, a_0 being the lattice parameter of the zinc blende structure. The first two terms in Eq. (1) do not depend on the σ's and define the potential of a lattice-periodic unperturbed system (the virtual crystal), whereas the third depends on the chosen configuration and will be treated by perturbation theory. The perturbation acting on the virtual crystal is the sum of neutral contributions localized at lattice sites, whose strength is proportional to the chemical difference between the atomic species, Ga and In. According to the sign of the σ's, each one of these *alchemic* perturbations "transforms" a virtual cation into a real Ga or In ion. Besides an electron-density response, this perturbation also induces a relaxation of the ions from their ideal positions, which is to leading order linear in its strength and can also be treated by perturbation theory. Using DFPT, the energy of the alloy is recast in the form [5]

$$E[\{\sigma_{\mathbf{R}}\}] = E_0 + K\sum_{\mathbf{R}} \sigma_{\mathbf{R}} + \frac{1}{2}\sum_{\mathbf{R}\mathbf{R}'} \sigma_{\mathbf{R}} J(\mathbf{R}-\mathbf{R}')\sigma_{\mathbf{R}'} + O(\Delta v^3), \quad (2)$$

where E_0 is the unperturbed energy, K—which is first order in the perturbation—acts essentially as a shift in the difference between the chemical potentials of the two pure compounds, and the interaction constants J are well-defined linear-response functions of the unperturbed virtual crystal. Neglecting atomic relaxation, the J would be very short ranged [5]; the effect of such relaxation is to renormalize the interaction constants via the term $J(\mathbf{R}-\mathbf{R}') \to J(\mathbf{R}-\mathbf{R}') - \sum_{\mathbf{R}'',\mathbf{R}'''} \boldsymbol{F}^T(\mathbf{R}''-\mathbf{R}) \cdot \Phi^{-1}(\mathbf{R}''-\mathbf{R}''') \cdot \boldsymbol{F}(\mathbf{R}'''-\mathbf{R}')$, where Φ is the matrix of the interatomic force constants, $F_{\alpha\delta}(\mathbf{R})$ is the αth component of the force acting on the δth virtual atom of the unit cell ($\delta = 1, 2$) located at $\mathbf{R}$ when the virtual ion at the origin is transformed into a real one, and the scalar products run over the six values of the $\{\alpha\delta\}$ indices. The dependence of the sound velocities upon direction determines a nonanalytic behavior of the inverse dynamical matrix at $\mathbf{q} = 0$ in reciprocal space, which results in a slow anisotropic decay of the renormalized J at large distances in real space [$J(\mathbf{R}) \sim 1/R^3$] [7]. The nature of this behavior is purely elastic, and the polarity of the material (which enters the dynamical matrix via the effective charges) does not affect it directly.

The dependence of the equilibrium volume upon composition, i.e., the *macroscopic* relaxation, is included, as is the *microscopic* relaxation, in the renormalization of the interaction constants and could be determined by an appropriate long-wavelength expansion of the energy. It is, however, more convenient and accurate to separate the two effects. To this end, an *elastic* contribution to the alloy formation enthalpy is defined as the energy needed to bring the individual pure materials from their equilibrium volumes, $\Omega_{\mathrm{GaP,InP}}$, to the alloy volume Ω: $\Delta E_{\mathrm{elast}}(x,\Omega) = x[E_{\mathrm{GaP}}(\Omega) - E_{\mathrm{GaP}}(\Omega_{\mathrm{GaP}})] + (1-x)[E_{\mathrm{InP}}(\Omega) - E_{\mathrm{InP}}(\Omega_{\mathrm{InP}})]$. This elastic energy can be calculated exactly from the equations of state of the two components, accounting thus for some additional anharmonicity. The *configurational* contribution to the formation enthalpy—i.e., the difference between the formation enthalpy and the elastic term—is then calculated from Eq. (2), where the interaction constants $J(\Omega)$, renormalized for $\mathbf{q} \neq 0$, depend explicitly on the volume Ω.

Our calculations have been performed in the local-density approximation to density-functional theory, using norm-conserving pseudopotentials and plane waves up to a kinetic-energy cutoff of 16 Ry; Brillouin-zone integrations have been performed using sets of $\mathbf{k}$ points equivalent to the ten Chadi-Cohen special points. The J have been calculated at the equilibrium volumes of GaP, InP, and of the virtual crystal ($x = 0.5$), and then quadratically interpolated in between.

The adequacy of second-order DFPT in describing the structure and the energetics of the alloy has been tested against nonperturbative calculations for the structures listed in Table I. In the bulk geometry, possible tetragonal distortions of the ordered structures are second order in the alchemic perturbation [8] and have been neglected (for the $SL[001]_{1+1}$ accurate calculations gave $c/a \sim 1.007$). All the structural properties are found to be in agreement up to a few thousandths of atomic units; the mean square error in the formation enthalpies is 2.2 meV/atom. The discrepancies are mainly due to the relevance of three-body contributions in the cluster expansion of the energies of the luzonite and famatinite structures; the inclusion of a three-body nearest-neighbors term in Eq. (2), fitted to the formation enthalpies of those structures, would decrease the mean square error to 1.1 meV/atom. This level of reliability for DFPT is well within the overall accuracy of first-principles calculations, as it results from a comparison among several calculations [4(b),9] performed with a variety of different technical ingredients (all-electron methods vs different pseudopotentials, parametrization of the exchange-correlation energy, $\mathbf{k}$-point sampling, and so on).

TABLE I. Lattice parameters (a.u.) and formation enthalpies ΔH (meV/atom) for different structures of $Ga_xIn_{1-x}P$, as obtained from DFPT. The fully self-consistent results are shown, in parentheses, for a comparison. "Bulk" refers to the free-standing alloy and "Epitaxial" to the alloy grown onto a GaAs substrate. The denominator in the Ga composition indicates the number of cations in the unit cell.

Structures		Bulk (a)			Epitaxial (b)		
	x_{Ga}	a_0	ΔH		$a_\perp$	ΔH	
$SL[001]_{1+1}$	1/2	10.61	21.4	(20.5)	10.61	0.8	(-0.2)
Luzonite	3/4	10.42	16.2	(18.1)	10.25	-0.9	(1.0)
Luzonite	1/4	10.79	16.8	(13.7)	10.98	1.9	(-1.1)
Chalcopyrite	2/4	10.60	10.3	(8.4)	10.60	-10.3	(-12.0)
Famatinite	3/4	10.42	9.1	(10.8)	10.25	-6.9	(-5.4)
Famatinite	1/4	10.79	11.8	(8.2)	10.97	-3.2	(-6.6)
$SL[111]_{1+1}$	1/2	10.61	31.1	(30.4)	10.63	10.6	
Random	0.5	10.60	18.3		10.61	-2.3	
α-phase	12/16	10.42	7.5	(8.6)	10.24	-8.3	
β-phase	26/32	10.38	6.2		10.16	-6.7	

We have then performed Monte Carlo (MC) simulations at the conditions of fixed pressure, temperature, and difference in the chemical potentials $\Delta\mu$, with a cell of 1024 atoms and periodic boundary conditions. In Fig. 1 we display the bond-length distributions for different Ga concentrations as obtained from simulations at the temperature of 1000 K, at which the alloy is miscible and random. A bimodal pattern clearly emerges, characterized by individual bond lengths (Ga-P and In-P) which are close to their pure-compound values and significantly different from the average, a characteristic feature of semiconductor alloys [10]. Our results are in close agreement with the experimental data [11], with a 1% offset due to the difference between the experimental and theoretical values of the bulk lattice parameters. The average lattice parameter of the alloy resulting from these simulations (full line) closely follows the linear behavior observed experimentally (Vegard's law); this result is by

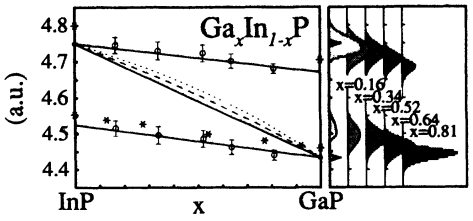

FIG. 1. Left panel: dependence of the bond lengths upon composition for bulk $Ga_xIn_{1-x}P$ at 1000 K (empty dots, with error bars for the variance and best-fit solid lines); experimental data are marked by asterisks. The average lattice parameter, scaled to the bond length, is also shown for the present (solid line) and other approximate approaches (dashed and dotted lines; see text). Right panel: bond-length distributions corresponding to several compositions; the arrows indicate the pure-compound bond lengths.

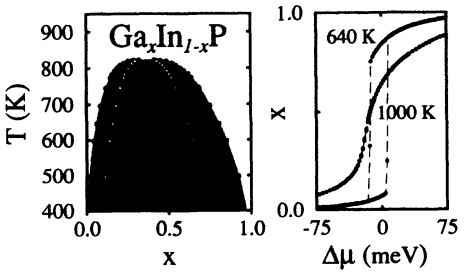

FIG. 2. Left panel: phase diagram of bulk $Ga_xIn_{1-x}P$. The solid line (filled circles) is the coexistence curve; the dashed one (empty circles) is the spinodal. Right panel: dependence of the average composition upon the chemical potential difference.

no means trivial and comes from an accurate balance between microscopic and macroscopic relaxation effects. In fact, if we had neglected the effects of disorder on the average lattice constant (taking the lattice constant of the concentration-weighted virtual crystal) or the dependence of the interaction constants upon volume, we would have obtained significant deviations from Vegard's law (dotted and dashed lines, respectively).

In order to determine the composition-temperature phase diagram, the Gibbs free energy is calculated via a thermodynamic integration [12]: the dependence of the average composition x on $\Delta\mu$ at any given temperature is obtained from two sequences of simulations performed for increasing and decreasing values of $\Delta\mu$ (right panel of Fig. 2); this relation is then inverted and integrated in order to obtain the relative free energies of the GaP-rich and InP-rich phases. The phase diagram is extracted determining the common tangent (that gives the coexistence line) and the inflection points (spinodal line) of the free energy curve [13]. The system presents a model random alloy behavior with a miscibility gap below a critical temperature of $T_c \sim 820$ K, corresponding to a critical composition $x_c \sim 0.4$ (left panel of Fig. 2). The role of the lattice mismatch (7% in the present case) is foremost in determining the phase stability, due to the dominant elastic term in the alloy formation enthalpy.

The critical temperature and composition estimated from experimental data [14] are $T_c^{\rm exp} \sim 930$ K, and $x_c^{\rm exp} \sim 0.6$. Zunger and co-workers [4(b)]—who included three- and four-body terms in their cluster expansion for the energy—obtained a closer agreement with these estimates. Many-body terms can be included in our scheme, either by pushing perturbation theory to higher orders or by fitting some of them to self-consistent calculations, in the spirit of a cluster expansion; we thus examined the effect of our neglect of many-body interactions on the alloy phase diagram. At the mean-field level, the introduction of the three-body nearest-neighbors interaction mentioned above resulted in the lowering of $T_c^{\rm MF}$ from 940 to 900 K and a shift of $x_c^{\rm MF}$ from ~ 0.40 to ~ 0.47. Although the disagreement with experimental data is thus reduced, we decided to maintain our original perturbative approach based on the full two-body expansion of the configurational energy [Eq. (2)] in view of its simplicity and of the large uncertainties which affect the experimental data [14]. The latter are in fact obtained from an extrapolation towards the interface of the concentration gradients in a segregated sample where the two phases are still inhomogeneous.

All the formation enthalpies listed in Table I(a) for the bulk (free-standing) alloy are positive, reflecting instability with respect to segregation; a few structures are, however, more stable than the corresponding disordered alloy. Therefore, in free-standing $Ga_xIn_{1-x}P$, spontaneous ordering is favored at low temperatures with respect to the random alloy, but taken over by the tendency towards segregation which is induced by the large elastic energy term. If segregation is inhibited in some way, some ordered structures can appear at low temperatures as metastable phases. This can be simulated in a MC run by umbrella sampling a narrow window around a given composition. For example, we were able to observe the formation of chalcopyrite for $T \lesssim 150$ K upon slow annealing from a homogeneously random sample.

When the alloy is pseudomorphically grown on a substrate with a different lattice parameter, the resulting strain has the effect of stabilizing some ordered structures with respect to segregation [2]. This is shown in Table I(b) where the formation enthalpies of the structures previously considered are now calculated supposing that the in-plane lattice constant is constrained to that of a GaAs substrate ($a_{\parallel} = 10.60$ a.u.) [15]. We see that in this case not only are some ordered structures more stable than the corresponding random alloy, but they are more stable even with respect to segregation; we expect therefore the appearance of spontaneous ordering in the epitaxial phase diagram of $Ga_xIn_{1-x}P$. In order to substantiate this hypothesis, we have performed MC simulations for $Ga_xIn_{1-x}P$ epitaxially constrained on a GaAs (001) substrate, following the same approach used for the free-standing alloy. The upper panels of Fig. 3 display, for two selected temperatures, the dependence upon $\Delta\mu$ of

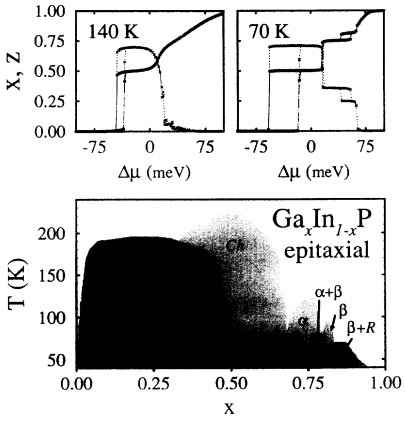

FIG. 3. Upper panels: dependence of the average composition (x, full circles) and of the chalcopyrite order parameter (z, crosses) upon the chemical potential difference for two different temperatures. Lower panel: phase diagram of $Ga_xIn_{1-x}P$ grown epitaxially on a GaAs (001) substrate. The white region corresponds to a homogeneous random phase (R); regions where one homogeneous ordered phase (chalcopyrite, α, or β) is stable are lightly shaded and regions where two phases coexist are shaded in a darker tone.

the average Ga concentration, x, and of the chalcopyrite order parameter, z; the latter is defined as the modulus of the relevant Fourier coefficient—in the $\langle 1\frac{1}{2}0\rangle$ star—of the real-space density function $\langle\sigma_{\mathbf{R}}\rangle$. At $T = 140$ K an hysteresis cycle is clearly visible, corresponding to the region of the phase diagram (indicated by "$R+Ch$" in Fig. 3) where the alloy segregates in a chalcopyrite and an In-rich random phase. On the right of the hysteresis cycle z remains large, identifying a region (designated by "Ch") where a homogeneous chalcopyrite is the stable phase. At a lower temperature (70 K) the phase diagram becomes richer, with several miscibility gaps corresponding to different phases at $\sim 50\%$, $\sim 75\%$, and $\sim 81\%$ compositions. The low-temperature phases can be nucleated by annealing the system in the appropriate range of chemical potential differences, without any further constraint; as expected, we found that the favored structure at $x = 0.5$ is the chalcopyrite. In addition, unexpected new ordered structures were identified for $x = 0.75$ and $x = 0.8125$; these are listed in Table I and indicated in Fig. 3 with labels α and β, respectively. These new phases are closely related to chalcopyrite and can be obtained from it by periodically substituting a few In atoms with Ga ones. In the lower panel of Fig. 3 we sketch the main features of the epitaxial phase diagram, as obtained by the analysis of the dependence upon $\Delta\mu$ of the average concentration and of the different order parameters corresponding to the three ordered structures. Finally, to double-check the overall reliability of our findings, we have compared the formation enthalpy of the cubic α phase as obtained from a fully self-consistent calculation with our DFPT results. The two calculations agreed within 1.1 meV/atom, which is again within the typical accuracy of DFPT.

Nicola Morzari received support as a Fellow of the Commission of the European Communities, Human Capital and Mobility program.

* Present address: SISSA, Trieste, Italy.

[1] *Metalorganic Vapor Phase Epitaxy 1988*, section *Ordered Phases* [J. Cryst. Growth. **93**, 396 (1988)]; A. Zunger and D.M. Wood, J. Cryst. Growth **98**, 1 (1989); G.B. Stringfellow, *ibid.* **98**, 108 (1989).

[2] J.L. Martins and A. Zunger, Phys. Rev. Lett. **56**, 1400 (1986); C.P. Flynn, *ibid.* **57**, 599 (1986); D.M. Wood and A. Zunger, Phys. Rev. B **40**, 4062 (1989).

[3] G.S. Chen and G.B. Stringfellow, Appl. Phys. Lett. **59**, 324 (1991); J.E. Bernard, S. Froyen, and A. Zunger, Phys. Rev. B **44**, 11 178 (1991); T. Suzuki and A. Gomyo (unpublished).

[4] (a) L.G. Ferreira, S-H. Wei, and A. Zunger, Phys. Rev. B **40**, 3197 (1989); (b) S-H. Wei, L.G. Ferreira, and A. Zunger, *ibid.* **41**, 8240 (1990); (c) D.B. Laks, L.G. Ferreira, S. Froyen, and A. Zunger, *ibid.* **46**, 12 587 (1992).

[5] S. de Gironcoli, P. Giannozzi, and S. Baroni, Phys. Rev. Lett. **66**, 2116 (1991); S. Baroni, S. de Gironcoli, and P. Giannozzi, in *Structural and Phase Stability of Alloys*, edited by J.L. Morán, F. Mejia-Lira, and L.M. Sanchez (Plenum Press, New York, 1992), p. 133.

[6] A. Gomyo, T. Suzuki, and S. Iijima, Phys. Rev. Lett. **60**, 2645 (1988); M. Kondow, H. Kakibayashi, T. Tanaka, and S. Minagawa, *ibid.* **63**, 884 (1989).

[7] N. Marzari and S. Baroni (unpublished).

[8] M. Peressi and S. Baroni, Phys. Rev. B (to be published).

[9] J.S. Nelson and I.P. Batra, Phys. Rev. B **39**, 3250 (1989); P. Bogusławski and A. Baldereschi, Phys. Rev. B **39**, 8055 (1989); R.G. Dandrea, J.E. Barnard, S.-H. Wei, and A. Zunger, Phys. Rev. Lett. **64**, 36 (1990); S.-H. Wei, L.G. Ferreira, and A. Zunger, Phys. Rev. B **41**, 8240 (1990); S.-H. Wei, L.G. Ferreira, J.E. Bernard, and A. Zunger, Phys. Rev. B **42**, 9622 (1990); C.H. Park and K.J. Chang, Phys. Rev. B **45**, 11 775 (1992).

[10] J.C. Mikkelsen, Jr. and J.B. Boyce, Phys. Rev. B **28**, 7130 (1983).

[11] Y. Takeda, H. Yamaguchi, and H. Oyanagi, in *Gallium Arsenide and Related Compounds 1991*, IOP Conf. Proc. No. 120 (Institute of Physics and Physical Society, London, 1992), p. 371.

[12] K. Binder, in *Festkörperproblem*, edited by P. Grosse (F. Vieweg, Braunschweig, 1986), Vol. 26, p. 133.

[13] D. de Fontaine, in *Solid State Physics*, edited by H. Ehrenreich, F. Seitz, and D. Turnbull (Academic, New York, 1979), Vol. 34, p. 150.

[14] K. Ishida, T. Nomura, H. Tokunaga, H. Ohtani, and T. Nishizawa, J. Less-Common Met. **155**, 193 (1989).

[15] We have assumed for this case that the interaction constants $J(a_\parallel, a_\perp)$ depend on the unit cell geometry only through the volume Ω; the error introduced by this "cubic" approximation in the configurational energies is negligible. The elastic energy terms have been calculated considering the dependence of the energy on both the volume and the tetragonal strain.

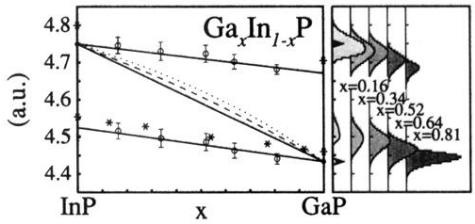

FIG. 1. Left panel: dependence of the bond lengths upon composition for bulk $Ga_xIn_{1-x}P$ at 1000 K (empty dots, with error bars for the variance and best-fit solid lines); experimental data are marked by asterisks. The average lattice parameter, scaled to the bond length, is also shown for the present (solid line) and other approximate approaches (dashed and dotted lines; see text). Right panel: bond-length distributions corresponding to several compositions; the arrows indicate the pure-compound bond lengths.

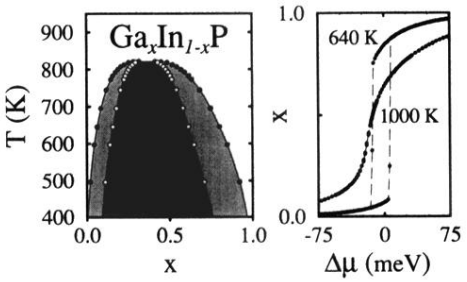

FIG. 2. Left panel: phase diagram of bulk $Ga_xIn_{1-x}P$. The solid line (filled circles) is the coexistence curve; the dashed one (empty circles) is the spinodal. Right panel: dependence of the average composition upon the chemical potential difference.

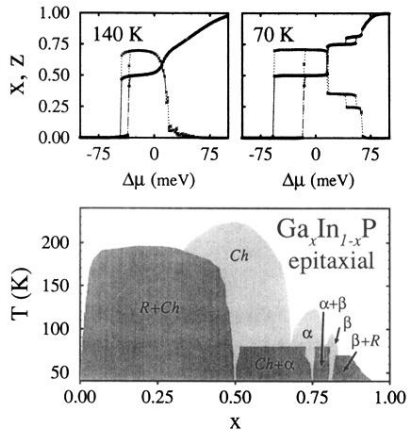

FIG. 3. Upper panels: dependence of the average composition (x, full circles) and of the chalcopyrite order parameter (z, crosses) upon the chemical potential difference for two different temperatures. Lower panel: phase diagram of $Ga_xIn_{1-x}P$ grown epitaxially on a GaAs (001) substrate. The white region corresponds to a homogeneous random phase (R); regions where one homogeneous ordered phase (chalcopyrite, α, or β) is stable are lightly shaded and regions where two phases coexist are shaded in a darker tone.